# Acoustic-radiation stress in solids. II. Experiment

W. T. Yost and John H. Cantrell, Jr.
*Langley Research Center, Mail Stop 231, National Aeronautics and Space Administration, Hampton, Virginia 23665*
(Received 14 February 1984; revised manuscript received 4 June 1984)

The first direct experimental evidence for the radiation-stress-induced static strain or displacement associated with the propagation of acoustic waves in solids is reported. Ultrasonic tonebursts launched into samples of single-crystal silicon along the [110] direction and vitreous silica (Suprasil W1) are seen to generate static displacement pulses having the shape of a right-angled triangle. This shape is in agreement with acoustic-radiation-stress theory which also predicts that the slope of the static displacement pulse depends directly on the magnitude and sign of the acoustic nonlinearity parameter of the solid. For silicon the nonlinearity parameter is positive and is seen to give rise to a dilative pulse, while for vitreous silica the nonlinearity parameter is negative and produces a contractive pulse as predicted. Calculations of the acoustic nonlinearity parameters from absolute measurements of the slope of the static displacement pulse and the amplitude of the ultrasonic toneburst yield the values 5.4 for silicon along the [110] direction and −12.7 for Suprasil W1. These values are in good agreement with those determined independently from ultrasonic harmonic-generation methods.

https://doi.org/10.1103/PhysRevB.30.3221

## I. INTRODUCTION

The radiation stress associated with elastic waves propagating in solids has been a subject that, in contrast to similar studies in liquids, has largely been neglected in the literature. Although similarities exist between acoustic wave propagation in liquids and in solids, fundamental differences also exist. For example, liquids do not support shear waves but solids do, and solids because of Poisson contraction are neither "laterally confined" nor "laterally unconfined" in response to acoustic wave propagation as is the case for liquids.[1] These differences result in intrinsically different expressions for the acoustic-radiation stress in the two media. In the preceding paper[2] (hereafter referred to as I) the radiation stress associated with acoustic wave propagation in solids of arbitrary crystalline symmetry is derived using two independent approaches and identical results are obtained. The derivation shows that the acoustic-radiation stress is composed of two contributions. One contribution results directly from the nonlinearity in the stress-strain (displacement-gradient) relationship. The second contribution, which is opposite in sign to the first, occurs from the linear term in the stress—displacement-gradient relationship as the result of the nonlinearity in the wave equation. The latter component gives rise to an acoustic-radiation-induced static strain in the solid.

Until now, experimental evidence for the existence of the acoustic-radiation-induced static strain has been indirect. Carr and Slobodnik[3] inferred the existence of the static strain in piezoelectric quartz and zinc oxide by measuring the dc voltage accompanying resonant acoustic static strain in thin disks of the sample material. Cantrell and Winfree[4] reported evidence of the static strain in single-crystal germanium by sinusoidally modulating the amplitude of a series of ultrasonic tonebursts launched into the solid and measuring the signal resulting from the static strain at twice the modulation frequency. In this paper we present the first direct experimental evidence of the acoustic-radiation-induced static strain. Critical features of the static waveform are found to be in agreement with the predictions in I.

## II. THEORETICAL CONSIDERATIONS

Consider a quantity $Q$ referred to the Lagrangian (material) coordinates. The time-averaged value of $Q$ at a given fixed point $a_1$ in those coordinates is defined by

$$\langle Q \rangle = \lim_{t\to\infty} \left[ \frac{1}{t} \int_0^t Q(a_1,t')dt' \right], \tag{1}$$

where $t$ is the time. The stress tensor $\sigma_{ij}$ in the Lagrangian frame is called the Boussinesq (or Piola-Kirchhoff) stress tensor and the time-averaged value $\langle \sigma_{ij} \rangle$ is called the Boussinesq radiation stress.

We consider in I a finite-amplitude acoustic wave propagating in direction $\vec{N}$ of a single crystal of arbitrary crystalline symmetry. Transforming coordinates in I such that the direction of wave propagation is along the $a_1$ axis of the transformed coordinate frame and diagonalizing the resulting expression, we obtain a decoupled equation relating the Boussinesq radiation stress $\langle \tau_{vq} \rangle$ in the transformed frame to the displacement gradients $\langle \partial P_j/\partial a_1 \rangle$ in that frame [Eq. (39) in I]. For an acoustic wave of polarization $j$ propagating in direction $\vec{N}$ we write

$$\langle \tau_{j1} \rangle = \mu_j \left[ \left\langle \frac{\partial P_j}{\partial a_1} \right\rangle - \tfrac{1}{2}\beta_j \left\langle \left[ \frac{\partial P_j}{\partial a_1} \right]^2 \right\rangle \right], \tag{2}$$

where $j = 1,2,3$ is the index of polarization corresponding to the one quasilongitudinal and two quasitransverse modes, $\mu_j$ is a linear combination of second-order elastic

coefficients, and $\beta_j$ is the $j$-mode acoustic nonlinearity parameter of the solid. The parameter $\beta_j$ characterizes the nonlinearity in the nonlinear wave equation

$$\frac{\partial^2 P_j}{\partial t^2}=c_0^2\left[1-\beta_j\frac{\partial P_j}{\partial a_1}\right]\frac{\partial^2 P_j}{\partial a_1^2}\,, \tag{3}$$

where

$$c_0=\left[\frac{\mu_j}{\rho_0}\right]^{1/2} \tag{4}$$

is the small amplitude wave velocity and $\rho_0$ is the mass density of the unperturbed solid.

We note from Eq. (2) that there are two contributions to the total Boussinesq radiation stress. The first term on the right-hand side of Eq. (2) results from the nonlinearity in the wave equation and gives rise to a radiation-induced static strain $\langle \partial P_j/\partial a_1\rangle$. The second contribution represented by $\langle(\partial P_j/\partial a_1)^2\rangle$ results from the nonlinearity in the stress-strain (displacement-gradient) relationship. In the experiments reported herein the measurement technique is sensitive only to the component which generates the radiation-induced static strain.

The relationship between the displacement gradient and the particle velocity is found in I [Eq. (34)] to be

$$\frac{\partial P_j}{\partial a_1}=-\frac{1}{c_0}\frac{\partial P_j}{\partial t}+\frac{\beta_j}{4c_0^2}\left[\frac{\partial P_j}{\partial t}\right]^2. \tag{5}$$

Substituting Eq. (5) into Eq. (1), we obtain

$$\left\langle\frac{\partial P_j}{\partial a_1}\right\rangle=\frac{\beta_j}{4c_0^2}\left\langle\left[\frac{\partial P_j}{\partial t}\right]^2\right\rangle=\frac{\beta_j}{4\mu_j}\langle E\rangle\,, \tag{6}$$

where in Eq. (6) we have used the boundedness of the displacement amplitude to set

$$\left\langle\frac{\partial P_j}{\partial t}\right\rangle=0\,, \tag{7}$$

and where to first order in the nonlinearity we have written the total-energy density $\langle E\rangle$ of the propagating wave as

$$\langle E\rangle=\rho_0\left\langle\left[\frac{\partial P_j}{\partial t}\right]^2\right\rangle. \tag{8}$$

These results are obtained in I [Eqs. (41) and (44)] using an approach based on the Fubini solution to the nonlinear wave equation. We see here that the same results are achieved without having to invoke solutions to the wave equation at all.

In the present experiments a purely sinusoidal acoustic wave of displacement amplitude $(P_j)_0$ and frequency $\omega$ is launched into the solid such that the boundary condition

$$P_j=(P_j)_0\sin(\omega t)\,,\quad a_1=0 \tag{9}$$

is satisfied. Since the total-energy density is conserved along the propagation path of the wave, we may write $\langle E\rangle$ in terms of the boundary state parameters as

$$\langle E\rangle=\tfrac{1}{2}\rho_0\omega^2(P_j)_0^2\,. \tag{10}$$

Substituting Eq. (10) into Eq. (6), we obtain

$$\left\langle\frac{\partial P_j}{\partial a_1}\right\rangle=\tfrac{1}{8}\beta_j\kappa^2(P_j)_0^2\,, \tag{11}$$

where $\kappa=\omega/c_0$ is the propagation number. We see from Eq. (11) that the acoustic-radiation-induced static strain is dependent upon the square of the frequency $\omega$ and the square of the initial wave displacement amplitude $(P_j)_0$. We also note a direct dependence on the acoustic nonlinearity parameter $\beta_j$. A positive value of $\beta_j$ produces a positive radiation-induced static strain and the solid must expand in the presence of a propagating acoustic wave. Similarly, a negative value of $\beta_j$ leads to a contraction (negative static strain) of the solid. Most solids of isotropic or cubic symmetry have positive nonlinearity parameters and, hence, expand in the presence of an acoustic wave. The only solid of isotropic or cubic symmetry we have been able to find having a negative $\beta_j$ is vitreous silica. Although other solids (perhaps of other symmetries) may be found to have a negative $\beta_j$, it appears they are relatively rare. The sign and magnitude of $\beta_j$ are important considerations in the experiments described.

Equation (11) is derived under the assumption of continuous wave propagation in infinite or semi-infinite solids. Let us consider the implications to an acoustic pulse or toneburst propagating in a finite solid. An acoustic toneburst of length $L$ and amplitude $(P_j)_0$ propagating in the solid from left to right is illustrated in Fig. 1(a). From Eq. (11) we see that the acoustic-radiation-induced static strain is defined only within the spatial extent $L$ of the acoustic toneburst, since $\langle E\rangle$ is nonzero only within that region. This results in the propagation of a flat-topped static strain pulse of amplitude $\langle \partial P_j/\partial a_1\rangle$ as shown in Fig. 1(b). The measurement technique we have used in the present work, however, is sensitive not to the strain amplitude of the propagating static waveform but rather to the displacement amplitude. We write the acoustic-radiation-induced static displacement amplitude $(P_j)_s$ at a position $a_s$ along the length of the pulse as

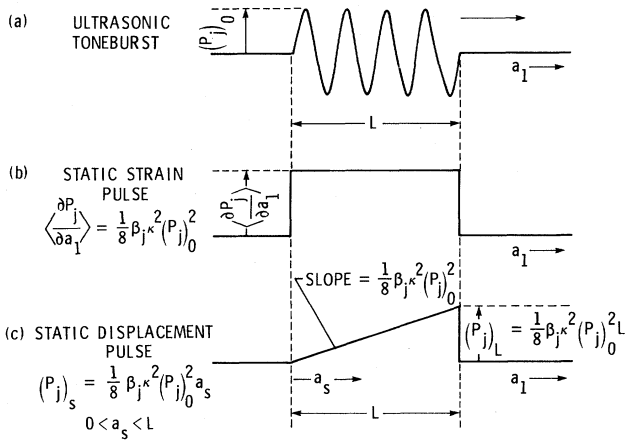


FIG. 1. Schematic of (a) acoustic toneburst, (b) acoustic-radiation-induced static strain pulse, and (c) acoustic-radiation-induced static displacement pulse.

$$(P_j)_s = \int_0^{a_s} \left\langle \frac{\partial P_j}{\partial a_1} \right\rangle da_1$$

$$= \tfrac{1}{8}\beta_j \kappa^2 (P_j)_0^2 a_s \ , \quad 0 \le a_s \le L \ . \tag{12}$$

We see from Eq. (12) that the shape of the radiation-induced static displacement pulse is that of a right-angled triangle or ramp propagating from left to right. The slope of the waveform is $\langle \partial P_j/\partial a_1 \rangle = \Delta(P_j)_s/\Delta a_s$ and the peak displacement amplitude $(P_j)_L$ is given by

$$(P_j)_L = \tfrac{1}{8}\beta_j \kappa^2 (P_j)_0^2 L \tag{13}$$

as shown in Fig. 1(c). Equation (13) indicates that the peak amplitude of the static displacement pulse increases linearly with the length $L$ of the toneburst.

In our experimental arrangement the acoustic toneburst is transmitted and received at opposite ends of the sample. As the static displacement pulse approaches the receiving end of the sample the maximum displacement amplitude (leading edge) of the pulse arrives first. This results in a mirror image of the static displacement waveform as illustrated in Fig. 2. We note that the slope of the ramp in Fig. 2 is

$$\frac{\Delta(P_j)_L}{\Delta t} = -\tfrac{1}{4}\beta_j \kappa^2 (P_j)_0^2 c_0 \ , \tag{14}$$

where the minus sign results from the mirror-image display, $t$ is time, and $c_0$ the small-amplitude sound wave velocity. The numerical factor in Eq. (14) is twice that of Eq. (11) because of the necessity of satisfying in our experiments a stress-free surface boundary condition at the receiving end of the sample.

## III. EXPERIMENTAL PROCEDURE

### A. Apparatus and measurement technique

A block diagram of the equipment arrangement used in the present experiments is shown in Fig. 3. A 30-MHz rf signal from a continuous-wave oscillator is combined in a mixer with a gating pulse from a logic and timing generator. The logic and timing generator counts down from the oscillator reference to time the generation of the gating pulse to the mixer. The length of the gating pulse is set such that the resulting gated rf signal from the mixer is composed of an integral number of 30-MHz cycles. Such an arrangement assures phase coherence of each rf pulse. The gated rf pulse is fed through a 8.5-MHz high pass filter to remove any leakage of the gating pulse through the mixer. The rf pulse is amplified by a 100-W broadband linear rf amplifier and is used to drive a 30-MHz narrow-band lithium niobate transducer bonded to one end of a cylindrical sample. The transducer generates a gated 30-MHz ultrasonic signal or toneburst which propagates through the sample. The toneburst is received by a broadband air-gap capacitive transducer at the opposite end of the sample.

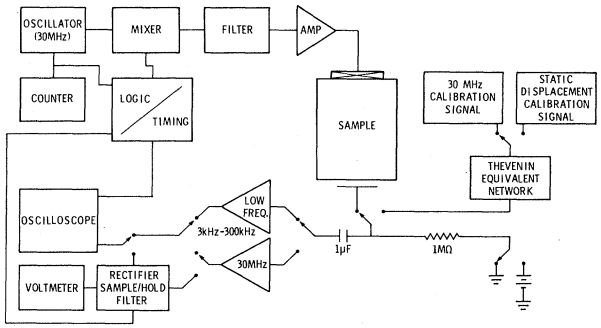


FIG. 3. Block diagram of equipment arrangement in present experiments.

The capacitive transducer is a parallel plate arrangement in which the sample end surface functions as the ground plate. The other plate is an optically flat electrode which is recessed approximately 7 $\mu$m from the sample surface. A dc bias of 50 V in our experiments is applied through a 1-M$\Omega$ resistor to the electrode. It has been shown[5] that the measurement of the output voltage from such a capacitive arrangement may be converted to a displacement measurement of the sample surface using the relation

$$V_d = V_b \frac{u}{s} \ , \tag{15}$$

where $V_d$ is the output voltage, $V_b$ is the dc bias voltage, $u$ is the displacement of the sample surface, and $s$ is the gap spacing between the capacitor plates. The capacitive transducer is capable of measuring[6] displacement amplitudes of the order $10^{-4}$ Å.

The present theory predicts that an acoustic toneburst propagating through a solid generates a radiation-induced static displacement pulse having the shape of a right-angled triangle. The slope of the triangular pulse is dependent upon the frequency and amplitude of the toneburst as well as the acoustic nonlinearity parameter of the solid. It is thus of interest to measure the amplitude of the 30-MHz toneburst as well as the slope of the static displacement pulse. The broad bandwidth of the capacitive transducer allows us to perform both measurements with the same experimental setup.

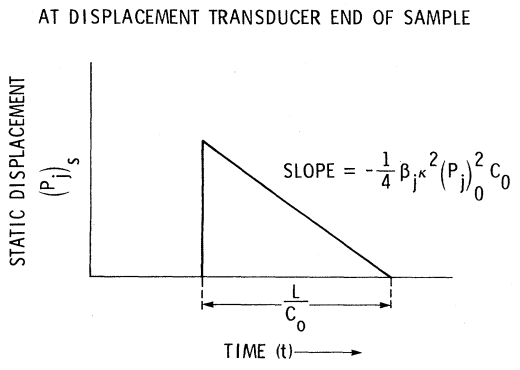


FIG. 2. Illustration of time-domain display of acoustic-radiation-induced static displacement signal at receiving end of sample.

*1. Measurement of toneburst amplitude*

The displacement amplitude of the 30-MHz toneburst is obtained by feeding the output from the capacitive transducer into a 30-MHz preamplifier (Fig. 3). The output from the preamplifier is sent into a rectifier and filter assembly which converts the 30-MHz toneburst into a detected signal. The rectifier and filter assembly also contains a sample and hold circuit which, when strobed, holds the voltage of the detected signal. The strobe signal is set by the logic and timing circuit and is adjusted to coincide with the center of the first toneburst through the sample following the electrical drive pulse to the transducer (i.e., the first ultrasonic echo). The output of the sample and hold is measured by a voltmeter and recorded.

The capacitive transducer is now switched out and a Thevenin equivalent network is switched into the circuit. The parameters of the Thevenin equivalent network are set to match the appropriate values of the capacitive transducer. The 1-MΩ resistor is removed from the bias source and that end grounded to prevent electrical surges through the circuits which may damage the instruments. A substitutional 30-MHz calibration signal is now switched into the Thevenin equivalent network and adjusted in amplitude until the voltmeter connected to the sample and hold reads the same value as that of the ultrasonic toneburst measurement. Since the amplitude of the 30-MHz calibration signal is measured at the input to the Thevenin equivalent network, the measured value is equal to the signal voltage produced by the capacitive transducer.

*2. Measurement of slope of static displacement pulse*

In order to display the acoustic-radiation-induced static displacement pulse the output of the capacitive transducer is connected to a Princeton Applied Research Model-113 low-frequency (3—300 kHz) preamplifier by a short, low-capacitance lead. The narrow bandwidth is necessary to reduce electrical noise in the measurement of the small static displacement signal. The output of the preamplifier is sent to an oscilloscope where the static displacement signal is displayed. A template is placed over the screen to record the static pulse shape.

The measurement of the slope of the static displacement pulse is performed by grounding the 1-MΩ bias resistor and switching to the Thevenin equivalent network. A calibration signal having the shape of a right-angled triangle is obtained from a Hewlett-Packard 3314A function generator and is connected to the Thevenin equivalent network. The amplitude and width (reciprocal frequency) of the calibration signal is adjusted until its slope is identical to that of the acoustic-radiation-induced static displacement pulse. The slope of the static displacement pulse is readily obtained from the measured calibration signal and is expressed in units of displacement per unit time using Eq. (15).

### B. Samples

Cylindrical samples of intrinsic single-crystal silicon along the [110] direction and vitreous silica (Suprasil W1) are used in the present experiments. The silicon sample is 3.0 cm in diameter, 3.8 cm in length, and the axial orientation is within ±2 degrees of the [110] direction. The Suprasil W1 sample is 3.8 cm in diameter and 2.2 cm in length. The discontinuity distances of the finite-amplitude acoustic waves used in the present experiments are calculated to be approximately 24 cm for silicon and 7 cm for Suprasil W1. The wave propagation distances in both samples are thus within the limits of the theory presented in I. The ends of each sample are parallel to within 12 arc seconds and are polished to $\frac{1}{5}$ wavelength of visible light. The sample ends are coated with chrome and gold to a thickness of 1000 Å. A 30-MHz compressional lithium niobate transducer (36°, $Y$ cut) is attached to one end of each sample using a phenyl salicylate bond. The sample is mounted in the capacitive transducer configuration described above by resting the free end of the sample on a ground ring assembly containing the recessed, electrically isolated electrode.

### C. Determination of the nonlinearity parameter

According to the present theory the acoustic nonlinearity parameter $\beta_j$ plays a dominant role in determining the amplitude and slope of the radiation-induced static displacement pulse. Its significance, however, extends beyond the present work. The nonlinearity parameter is a dimensionless measure of the anharmonicity of a crystal directly related to the mode Grüneisen parameters.[7] This anharmonicity is also responsible for the distortion of an acoustic wave propagating in a solid and the resulting harmonic generation. Since the amplitude of the harmonically generated waveform is directly dependent upon $\beta_j$, calculations of the nonlinearity parameters are commonly obtained from amplitude measurements of the fundamental and harmonically generated signals. The sign of $\beta_j$ in such measurements is determined using an independent phase detection technique.[8]

Since $\beta_j$ may also be determined from measurements of the slope of the static displacement pulse and the amplitude $(P_j)_0$ of the 30-MHz toneburst as described above, it is useful to compare measurements of $\beta_j$ using the two methods. We estimate the maximum experimental error in the present method of determining $\beta_j$ to be of the order 16%. This uncertainty is slightly higher than the 12% quoted for the harmonic-generation technique.[6] In contrast to the harmonic-generation technique, however, no independent measurement of the sign of $\beta_j$ is needed in the present method since the sign is determined at the time the slope measurement is made.

Measurement[9] of the acoustic nonlinearity parameter for single-crystal silicon along the [110] direction using the harmonic-generation technique yields the value 4.7. A similar measurement[10] for Suprasil W1 vitreous silica gives the value −11.6. We see then from Eqs. (11) and (12) that radiation-induced static displacement pulses of opposite polarity are expected to propagate in the two solids. A dilative pulse is predicted in silicon while a contractive pulse is predicted in Suprasil W1.

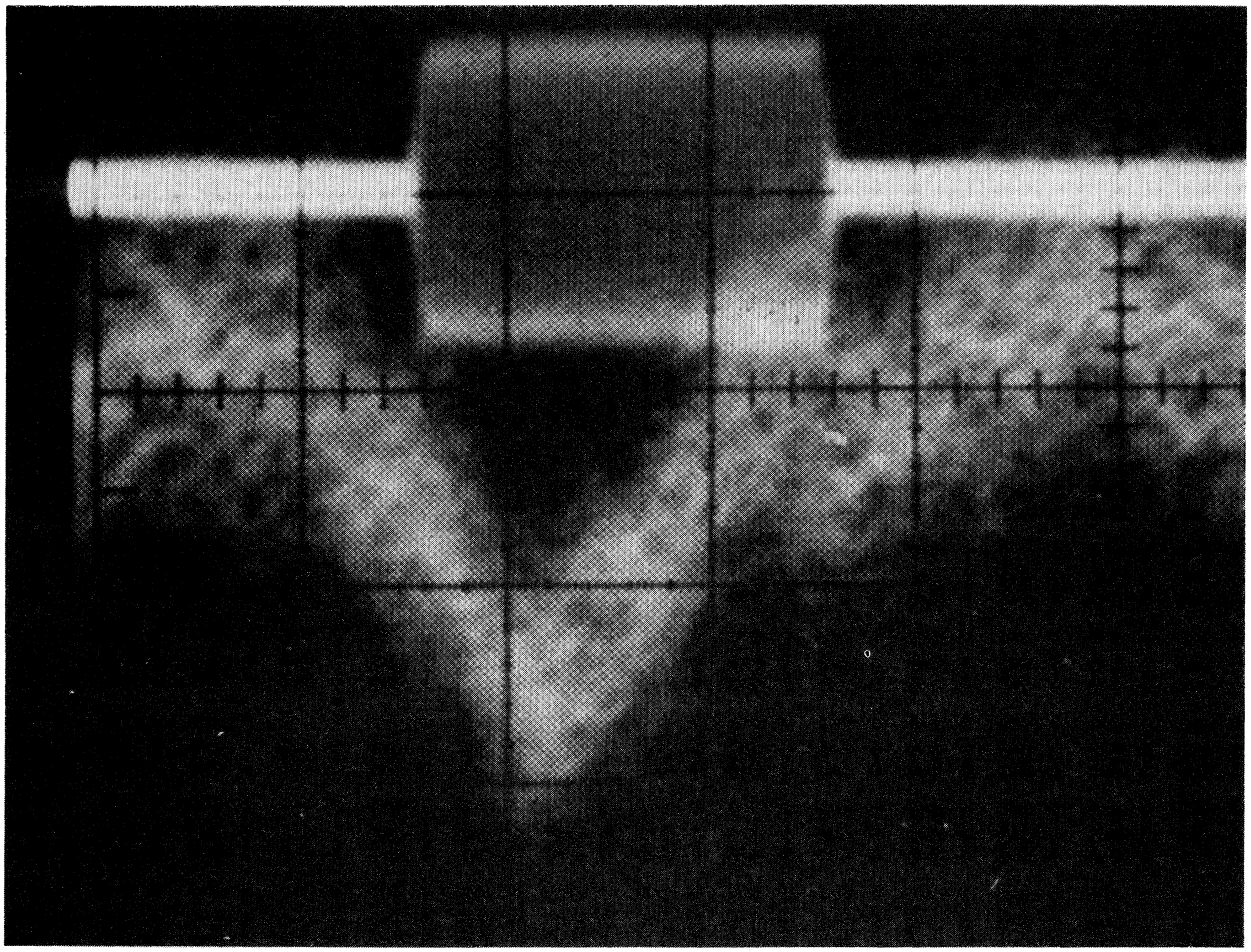

FIG. 4. Oscilloscope traces of 30-MHz toneburst (top) and acoustic-radiation-induced static displacement pulse (bottom) in single-crystal silicon.

## IV. EXPERIMENTAL RESULTS

An oscilloscope trace of the acoustic-radiation-induced static displacement pulse in the silicon sample is shown in Fig. 4. The 30-MHz toneburst is shown at the top; the static displacement pulse is displayed at the bottom. We note that the static displacement signal is negative and is in the shape of a right-angled triangle as predicted by theory. The slow risetime at the leading edge of the static pulse is due to the bandwidth limitations of the preamp. The slope of the static displacement signal, however, is within the bandwidth of the preamp. This together with the substitutional technique used in these experiments assures that the preamp bandpass is not a significant factor in the quantitative measurement of the slope.

In our experimental arrangement a negative static displacement signal indicates a dilation of the sample. This is an agreement with the theory for a solid having a positive value of the nonlinearity parameter $\beta_j$. The value of $\beta_j$ may be calculated from Eq. (14) using measurements of the slope of the static displacement pulse and the amplitude of the toneburst (measured to be $1.8\times10^{-9}$ m). The calculation yields a $\beta_j$ value of 5.4 for Si along [110]. As shown in Table I this value is consistent with that obtained from harmonic-generation measurements to within the experimental uncertainty of the measurement systems.

TABLE I. Comparison of acoustic nonlinearity parameters $\beta_j$ obtained in present work to those obtained from ultrasonic harmonic generation.

| | $\beta_j$ Present work | $\beta_j$ Harmonic generation | Author |
|---|---|---|---|
| Silicon along [110] | 5.4 | 4.7 | Philip and Breazeale[a] |
| Suprasil W1 | −12.7 | −11.6 | Cantrell and Breazeale[b] |

[a]Reference 9.
[b]Reference 10.

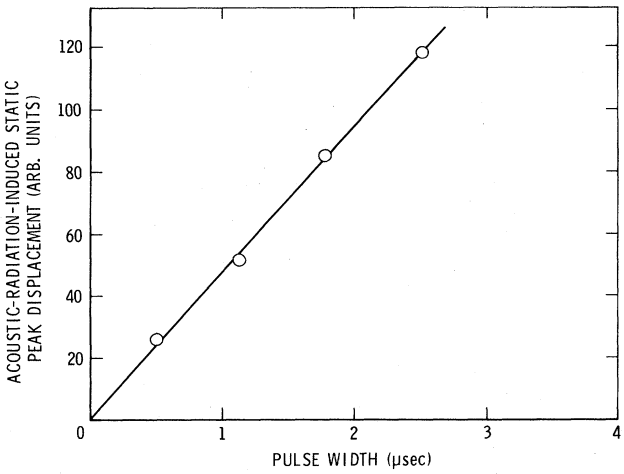


FIG. 5. Plot of acoustic-radiation-induced static peak displacement amplitude (ordinate) as a function of length of ultrasonic toneburst (abscissa).

According to Eq. (13) the peak displacement amplitude $(P_j)_L$ increases linearly with the length $L$ of the ultrasonic toneburst. In order to check this prediction we calibrated our measurement system by using a series of right-angled triangular waveforms from the function generator as the signal source of the Thevenin equivalent network. Each waveform has a different peak height but the slope was maintained at a value equal to that generated by the static displacement pulses in the silicon sample. The peak amplitude of each static displacement signal from the capacitance transducer was then compared to the corresponding calibration signal as a function of toneburst length. The peak displacement height for a pulse length of 2.7 $\mu$s, for example, is found to be $2.4\times10^{-11}$ m. The results of the relative measurements are shown in Fig. 5. The peak displacement amplitude (ordinate) is seen to increase linearly with the toneburst length (abscissa) as predicted.

Figure 6 shows the oscilloscope traces for the Suprasil W1 vitreous silica sample. The acoustic-radiation-

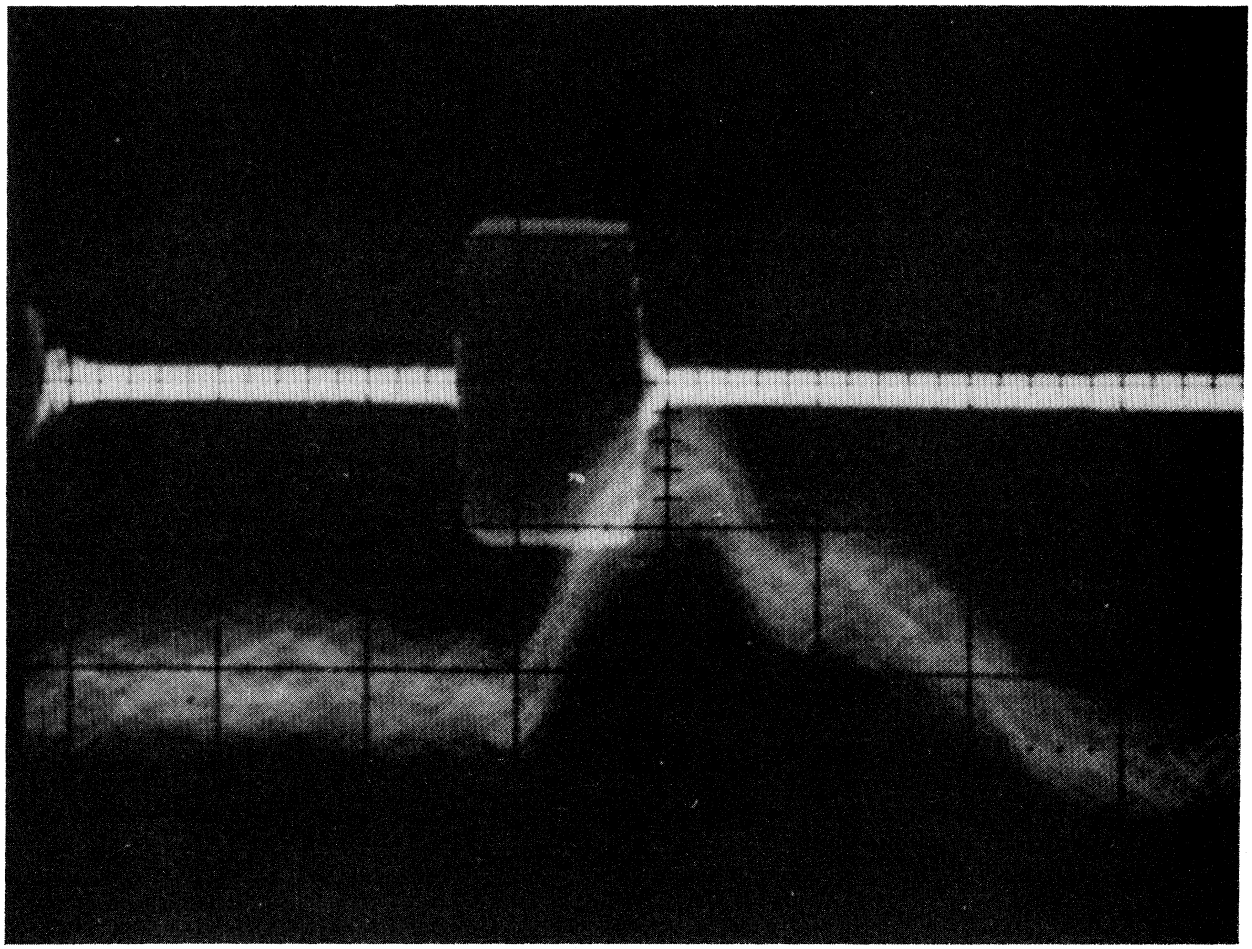

FIG. 6. Oscilloscope traces of 30-MHz toneburst (top) and acoustic-radiation-induced static displacement pulse (bottom) in Suprasil W1 vitreous silica.

induced static displacement signal is shown with the superposed 30-MHz toneburst. We note that the static displacement signal is now positive. The slope of the static displacement pulse while not uniquely defined here is, nonetheless, negative. A positive displacement signal in our experimental arrangement indicates a contraction of the sample. This is in agreement with the theory for a solid having a negative value of the acoustic nonlinearity parameter.

The appearance of a secondary peak in the static displacement pulse profile of Suprasil W1 introduces some ambiguity in the determination of $\beta_j$ from the slope measurements. Concomitant with the appearance of the secondary peak is an amplitude-dependent velocity dispersion. It is well known that such dispersion combined with nonlinearity in the waveform is inherent to the generation of solitary waves. We believe that the appearance of the two peaks in the displacement amplitude profile of Suprasil W1 is the result of the decomposition of the initial static displacement pulse profile into a finite train of solitons. A more complete investigation of this phenomenon is in progress.

We calculate the nonlinearity parameter using the slope associated with the first displacement peak shown in Fig. 6. This slope is chosen since the pulse width defined by extrapolation of a line having this slope from the first peak to the baseline most closely approximates the width of the toneburst. The amplitude of the toneburst is measured to be $1.2\times10^{-9}$ m and the peak static displacement amplitude is found to be $2.5\times10^{-11}$ m for a 1.8-$\mu$s pulse width. The calculation using Eq. (14) yields the value $-12.7$ for $\beta_j$. As shown in Table I this value is consistent with that obtained from harmonic-generation measurements.

## V. CONCLUSIONS

We have applied the theory in I of acoustic-radiation stress in infinite and semi-infinite solids to the case of spatially confined ultrasonic tonebursts propagating in solids of finite dimension. The theory predicts the existence of an acoustic-radiation-induced static displacement pulse having the shape of a right-angled triangle. The shape of the displacement pulse is predicted to be dependent upon the product of the energy density of the toneburst and the acoustic nonlinearity parameter of the solid. Our experiments show that the static displacement pulse for single-crystal silicon has the shape predicted by theory, but additional structure which we attribute to soliton generation is found for Suprasil W1 vitreous silica.

Quantitative confirmation of the theory is obtained from the calculation of the acoustic nonlinearity parameters of Si along [110] and Suprasil W1 using absolute measurements of the energy density of the toneburst and the slope of the static displacement pulse in each solid. Our calculations of the nonlinearity parameters are in agreement with those obtained from independent harmonic-generation measurements. The acoustic-radiation stress is found to generate a dilative pulse in silicon and a contractive pulse in Suprasil W1 as predicted in I. These results are the first direct experimental evidence of the existence of a radiation-stress-induced static strain associated with the propagation of an acoustic wave in a solid.

[1]B.-T. Chu and R. E. Apfel, J. Acous. Soc. Am. **72**, 1673 (1982); also, R. E. Apfel (private communication).
[2]J. H. Cantrell, Jr., preceding paper [Phys. Rev. B **30**, 3214 (1984)].
[3]P. H. Carr and A. J. Slobodnik, Jr., J. Appl. Phys. **38**, 5153 (1967).
[4]J. H. Cantrell, Jr. and W. P. Winfree, Appl. Phys. Lett. **37**, 785 (1980).
[5]W. B. Gauster and M. A. Breazeale, Rev. Sci. Instrum. **37**, 1544 (1966).
[6]W. T. Yost and M. A. Breazeale, Phys. Rev. B **9**, 510 (1974).
[7]J. H. Cantrell, Jr., Phys. Rev. B **21**, 4191 (1980).
[8]J. A. Bains, Jr. and M. A. Breazeale, J. Acoust. Soc. Am. **57**, 745 (1975).
[9]J. Philip and M. A. Breazeale, J. Appl. Phys. **52**, 3383 (1981).
[10]J. H. Cantrell, Jr. and M. A. Breazeale, Phys. Rev. B **17**, 4864 (1978).

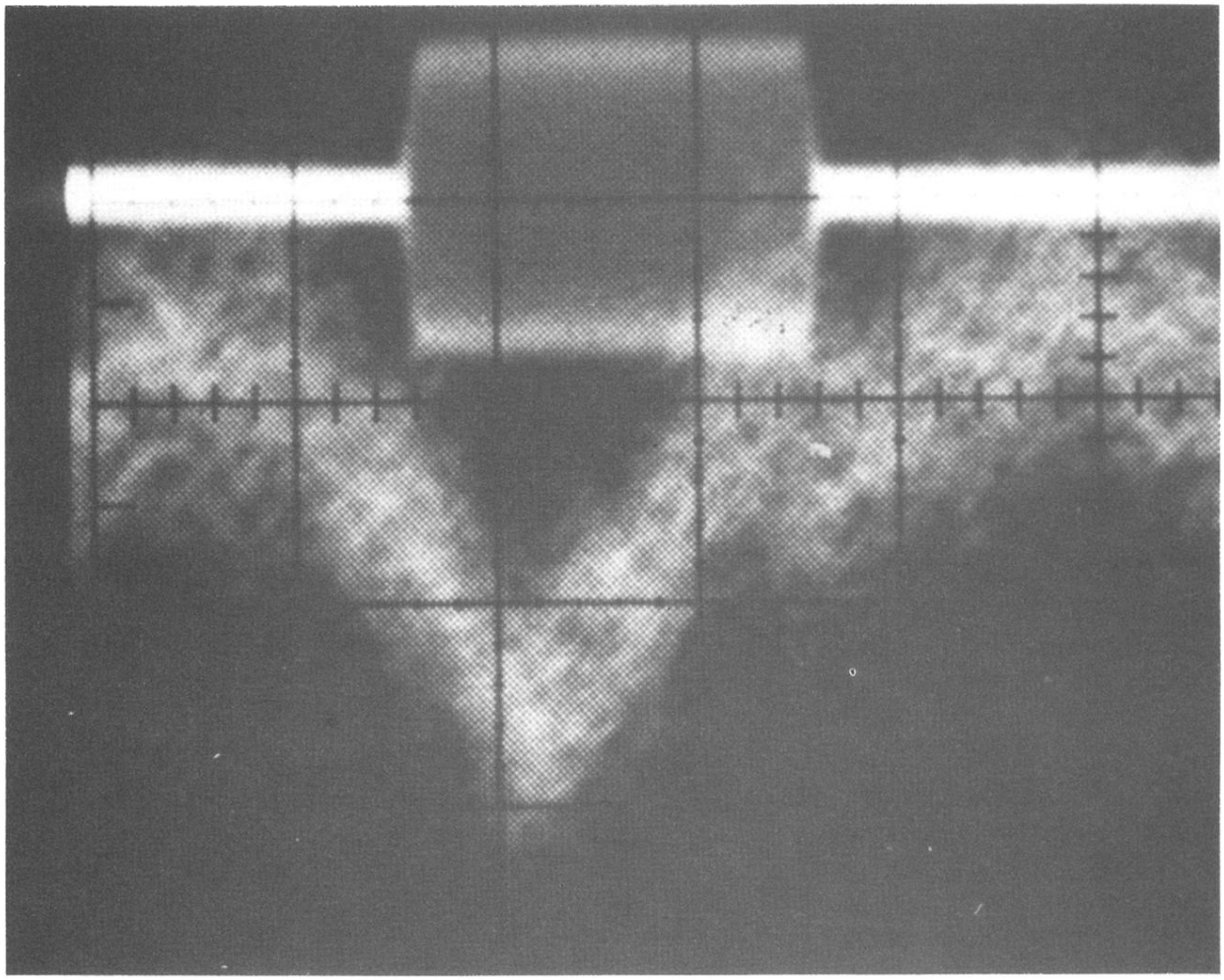

FIG. 4. Oscilloscope traces of 30-MHz toneburst (top) and acoustic-radiation-induced static displacement pulse (bottom) in single-crystal silicon.

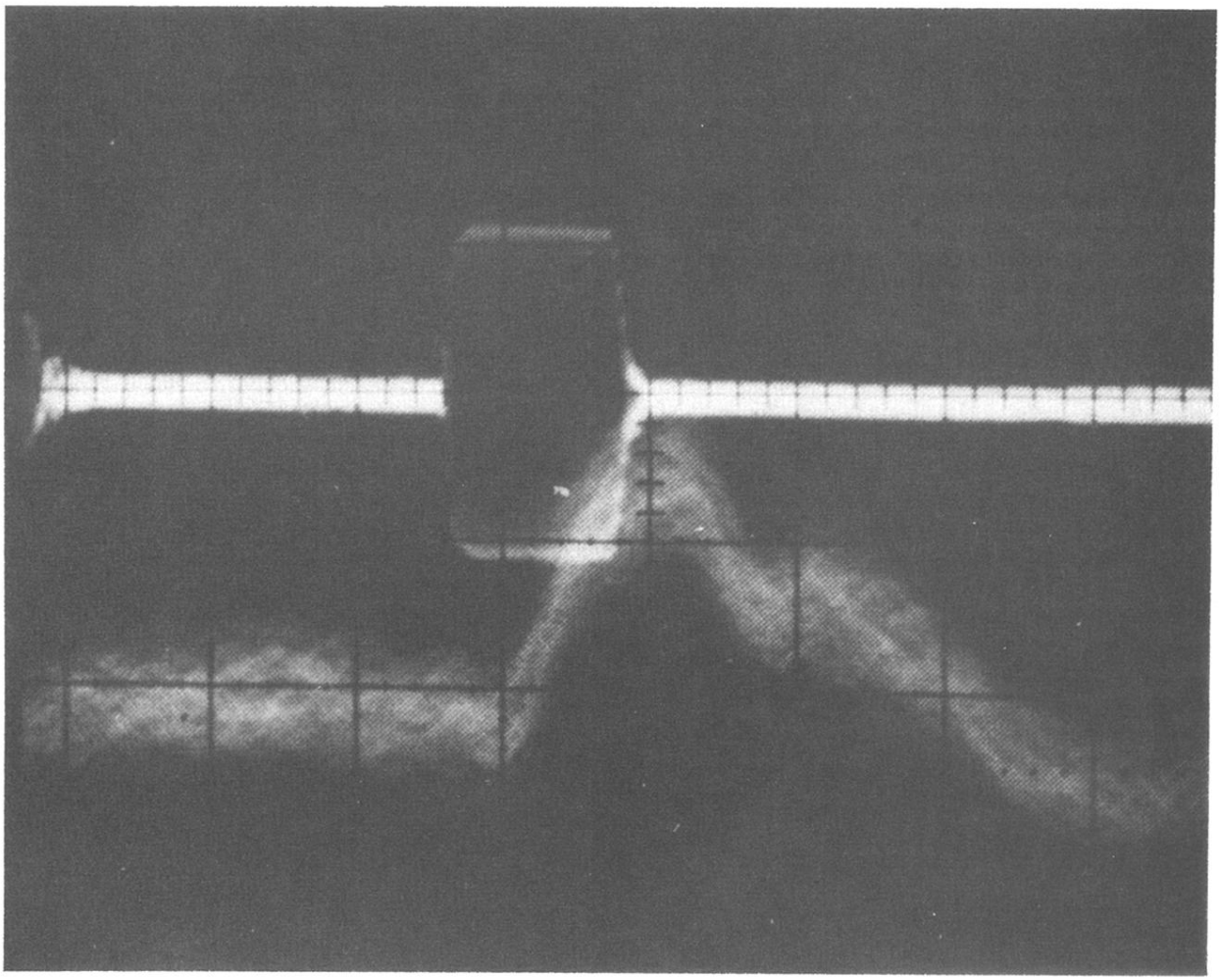

FIG. 6. Oscilloscope traces of 30-MHz toneburst (top) and acoustic-radiation-induced static displacement pulse (bottom) in Suprasil W1 vitreous silica.